Synthesis, and characterization of metal transition complexes derived from the Schiff base ligand *N*,*N*'-Bis(5-bromosalicylidene)-propane-1,2-diamine (H_2L)

ABSTRACT

Four new transition metal complexes [Mn(*L*)(Cl)] (**1**), [Fe(*L*)(Cl)] (**2**), [Co(*L*)(H_2O)$_2$] (**3**), [Ni(*L*)(H_2O)] (**4**) and [Cu(*L*)] (**5**), are synthesized from the Schiff base ligand *N*,*N*'-Bis(5-bromosalicylidene)-propane-1,2-diamine (H_2L) which derived from the condensation of 5-bromosalicylaldehyde with propane-1,2-diamine in methanol. The complexes are characterized by elemental analysis, FTIR and UV-visible spectroscopies, conductivity and magnetic moment measurements. The results show that the complexes **1**-**5** are mononuclear neutral electrolytes in DMF. The dinegative tetradentate ligand is coordinated to the metal ion through two phenolate oxygen atoms and two azomethine nitrogen atoms. Octahedral geometry is proposed for complex **3**, square planar geometry is proposed for complexes **4** and **5** and square pyramidal geometry is proposed for complex **1** and **2**. The structures of complexes **1** and **5** were solved by single crystal X-ray diffraction. Complex **1** crystallizes in a monoclinic system, with space group $P2_1/c$, while complex **5** crystallizes in a monoclinic system, with space group $C2/c$.

Keywords: Propane-1,2-diamine, 5-bromosalicylaldehyde, FTIR, UV-Visible, Complex, X-ray diffraction

1. INTRODUCTION

Schiff bases containing azomethine and phenoxy groups linked by an aliphatic chain are important precursors for obtaining coordination complexes whose fields of application are constantly expanding [1–5]. Although these ligands are widely studied, they continue to attract increasing interest thanks to the possibilities offered by organic chemistry [6–8]. Indeed, it is possible to functionalize the starting amines and ketones or aldehydes as well as the units linking them, the azomethine groups and the phenoxy groups [9–13]. Asymmetric Schiff bases offer more possibilities for building molecular structures, particularly in metalloproteins [14, 15] and asymmetric induction catalysis [16, 17]. Ligands with interesting properties such as chirality were developed and their ability to generate complexes with specific properties was studied [18–20]. The combination of these ligands with transition metals made it possible to generate new stable compounds. Transition metal complexes with these types of Schiff base ligands have found applications in the fields of biology [21], in the treatment of diseases such as cancers [22], malaria [23], bacterial [24] and viral [25] infections. These complexes are also used in fields such as computer science and electronics for their magnetic [26], luminescent [27] or optical [28] properties. We report here the synthesis of the chiral asymmetric ligand *N*,*N*'-Bis(5-bromosalicylidene)-(2-methyl)ethane-1,2-diamine (H_2L) derived from the precursor 5-bromosalicylaldehyde and propane-1,2-diamine having a N_2O_2 cavity and its complexes with transition metals (Scheme 1). The ligand allowed the synthesis of five new complexes whose structures are determined by a spectroscopic study (FTIR and UV-visible), conductimetric and magnetic moments measurements at room temperature of the complexes. The structure of the Mn(III) and the Cu(II) complexes were solved with single crystal X-ray diffraction technique.

2. MATERIAL AND METHODS

2.1 Starting materials and Instrumentations

5-bromosalicylaldehyde, propane-1,2-diamine, cobalt chloride hexahydrate, manganese chloride hexahydrate, iron chloride tetrahydrate, nickel chloride hexahydrate and copper chloride dihydrate were commercial products (from Aldrich) and were used without further purifications. The solvents were reagent grade and were purified by usual methods. Elemental analyses were carried out using a VxRio

EL Instrument. The FTIR spectra were recorded on a FTIR Spectrum Two of Perkin Elmer (4000–400 cm^{-1}). The UV–Visible spectra were run on a Perkin-Elmer UV/Visible spectrophotometer Lambda 365 (1000–200 nm). The ^{1}H and ^{13}C NMR spectra of the Schiff base were recorded in dmso-d_6 on a BRUKER 500 MHz spectrometer at room temperature using TMS as an internal reference. The molar conductance of 10^{-3} M solutions of the metal complexes in DMF were measured at 25 °C using a WTW LF-330 conductivity meter with a WTW conductivity cell. Magnetic measurements for complexes were performed at room temperature by using a Johnson Mattey scientific magnetic susceptibility balance (Calibrant: $Hg[Co(SCN)_4]$).

2.2 Synthesis of the ligand *N,N'*-Bis(5-bromosalicylidene)-(2-methyl)ethane-1,2-diamine (H_2L)

In a 100 mL flask, 10 mL of methanol and 5-bromosalicylaldehyde (2.5 g, 13.5 mmol) are introduced. Then, propane-1,2-diamine (0.5 g, 6.75 mmol) dissolved in 5 mL of methanol was added. The mixture was refluxed for three hours. The yellow solution obtained was placed in the refrigerator. After 48 hours, the yellow precipitate formed was recovered by filtration and washed with 2 x 10 mL of ethanol and then dried in the open air. Yield: 75.42%. M.P.: 114 °C.

2.3 Synthesis of the complexes

In a 100 mL flask, methanol (5 mL) and the ligand H_2L (0.1 g; 0.22 mmol) were introduced. A solution of $MCl_2{\cdot}n(H_2O)$ (0.22 mmol) in 5 mL of methanol (M=Cu, Ni, Mn, Co or Fe) was then added. The mixture was stirred at room temperature for one hour before filtration. The filtrate was left to evaporate slowly. After several days, the solid formed was recovered by filtration and washed with 2 x 10 mL of ether. The solutions of the copper and manganese complexes give crystals suitable for single-crystal XRD analysis.

2.4 X-ray structure determination of complex 2 and 5

Methanol solutions of **1** and **5** were left to slow evaporation and crystals suitable for X-ray analysis were formed after three weeks. Single Crystal X-ray Diffraction (SCXRD) data for both complexes were collected on a Rigaku XtaLAB Synergy-S Dualflex diffractometer equipped with an HyPix 6000HE detector, using Cu Kα (1.54184 Å) radiation. CrysAlisPro software was used for the data collection and reduction, cell refinement and absorption correction (Oxford Diffraction /Agilent Technologies UK Ltd. CrysAlisPro. at (2024)). The structures were determined using the intrinsic phasing method implemented in the SHELXT-2018/2 software (Sheldrick, G. M. SHELXT - Integrated space-group and crystal-structure determination. *Acta Crystallogr. Sect. A* **71**, 3–8 (2015)), and refined employing the least-squares method with SHELXL-2019 (Sheldrick, G. M. Crystal structure refinement with SHELXL. *Acta Crystallogr. Sect. C* **71**, 3–8 (2015).), both integrated within the Olex2 (Dolomanov, O. V, Bourhis, L. J., Gildea, R. J., Howard, J. A. K. & Puschmann, H. OLEX2: a complete structure solution, refinement and analysis program. *J. Appl. Crystallogr.* **42**, 339–341 (2009).) software platform. All non-hydrogen atoms were refined anisotropically, while hydrogen atoms were refined isotropically at idealized positions using the riding model. Graphical illustrations were generated using Olex2.

Table 1. Crystallographic data and refinement parameters for complexes 1 and 5.

Parameters	**1**	**5**
Chemical formula	$C_{17}H_{14}Br_2ClMn_2O_2$	$C_{17}H_{14}Br_2CuN_2O_2$
*M*r	528.51	501.66
Crystal system	Monoclinic	Monoclinic
Space group	$P2_1/c$	$C2/c$
Temperature (K)	210	100

a (Å)	13.8359 (4)	25.3523 (5)
b (Å)	9.5473 (3)	10.2283 (2)
c (Å)	14.6069 (5)	7.0358 (2)
β (°)	111.623 (4)	108.668 (2)
V (Å^3)	1793.72 (11)	1728.47 (7)
Z	4	4
Radiation type	Cu *K*α	Cu *K*α
μ (mm^{-1})	12.70	7.30
Crystal size (mm)	0.08 × 0.04 × 0.01	0.28 × 0.10 × 0.04
T_{min}, T_{max}	0.557, 0.942	0.571, 1.000
No. of measured reflections	19888	8961
No. of independent	3646	1642
No. of observed [$I > 2\sigma(I)$]	3321	1550
R_{int}	0.052	0.034
$R[F^2 > 2\sigma(F^2)]$	0.045	0.039
$wR(F^2)$	0.090	0.114
S	1.12	1.09
No. of reflections	3646	1642
No. of parameters/restraints	246/2	115/0
$\Delta\rho_{max}$, $\Delta\rho_{min}$ (e Å^{-3})	0.62, -0.49	0.94, -0.88

3. RESULTS AND DISCUSSION

3.1 General study

The ligand H_2L was prepared by a facile condensation of 5-bromosalicylaldehyde and propane-1,2-diamine in methanol (Scheme 1). The analytical data agree with the formulation (Table 2). The FTIR and UV-visible data are summarized in Table 3. The absence of bands characteristic of carbonyl and primary amine groups on the ligand spectrum, combined with the presence of a sharp band at 1629 cm^{-1} attributable to the valence stretching $\nu_{C=N}$ [32], shows that condensation has taken place. The broad band pointed at 3489 cm^{-1} corresponds to the ν_{O-H} of the phenolic hydroxy [33]. The phenolic ν_{C-O} band appears at 1278 cm^{-1} [34]. The ^{1}H NMR spectrum of the ligand H_2L shows a broad signal at 13.32 ppm in the form of a singlet integrating two protons attributed to the phenolic OH groups. The protons of the azomethine HC=N groups are identified in the form of two singlet integrating one proton each, respectively, at 8.55 and 8.58 ppm, confirming the asymmetry of the ligand. A complex multiplet signal integrating six aromatic protons is observed in the region of [6.82 – 7.65] ppm. The protons of the -CH_2-CH(Me)- chain are identified, in the form of a complex multiplet signal, integrating three protons in the region of [3.74 – 3.86] ppm.

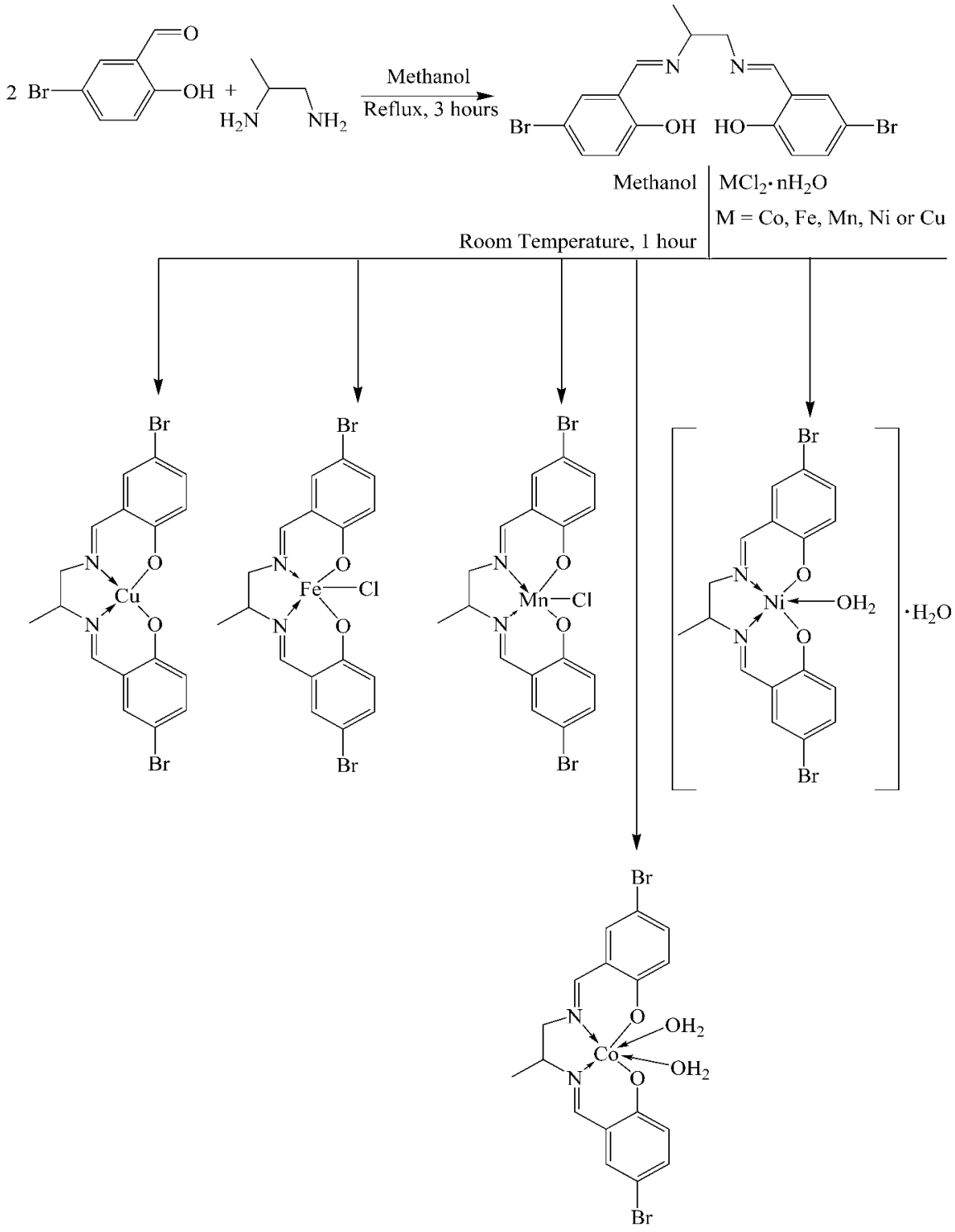

Scheme 1. Synthetic procedure of the ligand H_2L and its metal transition complexes.

The signal in the form of a doublet at 1.31 ppm integrating three protons is attributed to the CH_3- group. The ^{13}C NMR spectrum of the H_2L ligand is recorded in dmso-d_6. The signals due to the carbon atoms of the azomethine functions are located, respectively, at 166 and 164 ppm. The aromatic carbon atoms C_{ipso}-OH appear at 159.8 and 160.03 ppm, while the signals of the other aromatic carbon atoms appear in the range of 109 ppm to 134 ppm. The signals of the methylene and methynic carbon atoms appear at 64 and 63 ppm, respectively. The signal of the methyl carbon atom is located at 19 ppm.

Table 2. Analytical data for H_2L and complexes 1-5.

Complexes	Yield (%)	Color	% C Calc. (Found)	% H Calc. (Found)	% N Calc. (Found)	% Cl Calc. (Found)
H_2L	75.4	Yellow	46.39 (46.34)	3.66 (3.62)	6.36 (6.33)	-
[MnLCl] (**1**)	52.7	Brown	38.63 (38.60)	2.67 (2.64)	5.30 (5.27)	6.71 (6.24)
[FeLCl] (**2**)	44.5	Black	38.57 (38.53)	2.67 (2.63)	5.29 (5.25)	6.70 (6.65)
[CoL$(H_2O)_2$] (**3**)	55.8	Brown	38.30 (38.26)	3.40 (3.38)	5.26 (5.22)	
[NiL]·H_2O (**4**)	59.8	Orange	39.66 (39.63)	3.13 (3.09)	5.44 (5.40)	-
[CuL] (**5**)	59.6	Purple	40.70 (40.66)	2.81 (2.78)	5.58 (5.54)	-

Table 3. Main FTIR and UV-Visible data, room temperature magnetic moments and conductance of complexes 1-5.

Compound	ν(O-H)	ν(C=N)	ν(C-O)	λ(nm)	μ_{eff} (μ_B)	Λ ($\Omega^{-1}\cdot cm^2\cdot mol^{-1}$)
H_2L	3489	1630	1278	290, 340	-	-
[MnLCl] (**1**)	-	1620	1176	298, 347, 417	4.68	9.31
[FeLCl] (**2**)	-	1622	1178	331, 421, 505	5.7	8.67
[CoL$(H_2O)_2$] (**3**)	3368	1641	1176	296, 345, 407, 621, 988	4.62	11.4
[NiL]. H_2O (**4**)	3224	1622	1153	296, 341, 420, 559	diam	12.41
[CuL] (**5**)	-	1627	1177	293, 375, 580	1.6	4.51

The analytical data ofcompounds **1**-**5** agree with the formulation proposed for the complexes (Table 2). The main data of FTIR and UV-visible of the complexes are summarized in Table 3. The $\nu_{C=N}$ band of the free ligand located at 1629 cm^{-1} undergoes, after complexation, a shift towards low frequencies for complexes **1**, **2**, **4** and **5** and a shift towards high frequencies for complex **3**. These observations indicate the involvement of the nitrogen atoms of the azomethine groups in the coordination of the metal [34]. The ν_{C-O} vibration band, which appears at 1278 cm^{-1} on the spectrum of the free ligand, also shifts towards low frequencies for complexes **1**-**5**. We also note the disappearance of the ν_{O-H} vibration band which was located at 3489 cm^{-1} on the spectrum of the free ligand. These two facts indicate the involvement of the oxygen atoms in their phenolate forms in the coordination with the metal center [35]. For cobalt (**3**) and nickel (**4**) complexes, the broad and intense vibration bands pointed at 3368 cm^{-1} and 3224 cm^{-1}, respectively, suggest the presence of water molecules [36]. Conductance measurements of millimolar solutions of the complexes were taken in DMF. All complexes **1**-**5** exhibit low molar conductivity (4.51-12.41 $\Omega^{-1}\cdot cm^2\cdot mol^{-1}$) (Table 3), corresponding to neutral electrolytes [37]. After fifteen days, these values remain almost constant, indicating good stability of the complexes in DMF. The UV-visible spectrum of the free ligand shows two bands at 290 and 340 nm, which are attributed to the $\pi\rightarrow\pi^*$ and $n\rightarrow\pi^*$ transitions of the aromatic groups, the azomethine and the phenol chromophores, respectively. The UV-visible spectra of the complexes are recorded in millimolar solution in DMF. The

spectra of the manganese (**1**), cobalt (**3**), nickel (**4**) and copper (**5**) complexes, show electronic absorptions in the ranges [293-298] nm and [341-375] nm attributed, respectively, to the $\pi \rightarrow \pi^*$ and $n \rightarrow \pi^*$ transitions in the aromatic rings, the azomethine groups and the phenolate groups [38]. For complexes **1**, **3**, **4** and **5**, the absorption bands in region 407-421 nm are due to charge transfer from the ligand to the metal (LMCT) [39]. In the case of complex **2**, the observed band at 505 nm is attributed to charge transfer from the ligand to the Fe(III) ion [40]. The UV-visible spectra of the manganese (**1**) and iron (**2**) complexes do not show bands attributable to d→d transitions. The effective magnetic susceptibility value of the manganese complex (**1**) which is 4.68 µB at room temperature is close to the value reported for a spin-only d^4 Mn(III) ion in a square pyramidal environment [41]. The iron complex (**2**) has a magnetic moment of 5.7 µB which suggests that the compound is a mononuclear complex in which the Fe(III) ion is located in a square pyramidal environment. Indeed, high-spin Fe(III) in a square pyramidal environment gives a spin-only magnetic moment value of 5.92 µB [42]. The starting Mn(II) and Fe(II) ions underwent aerobic oxidation to give Mn(III) and Fe(III) ions, respectively, during the complexation reaction with the ligand [40]. In the case of the manganese complex these observations are confirmed by XRD structure determination. The UV spectrum of the cobalt complex (**3**) reveals, also, absorption bands centered at 988 and 621 nm, which are attributed to the $^4T_{1g}(F) \rightarrow {}^4T_{1g}(P)$ and $^4T_{1g}(F) \rightarrow {}^4T_{2g}(F)$ transitions, respectively. These absorption bands, together with the magnetic moment value of 4.62 µB, indicate an octahedral environment around the Co(II) ion [43]. The spectrum of the nickel complex shows a single absorption band in the visible region at 559 nm. Nickel complexes exhibit two allowed bands at, approximately, 450 and 550 nm due to the $^1A_{1g} \rightarrow {}^1A_{2g}$ and $^1A_{1g} \rightarrow {}^1B_{1g}$ transitions for a Ni(II) complex in which the metal ion is located in a square planar environment [44]. Additionally, the measurement of the magnetic susceptibility shows that complex **4** is diamagnetic, confirming the square planar geometry around Ni(II) [45]. On the spectrum of the copper complex, the d→d band pointed at 580 nm corresponds to the $^2B_{1g} \rightarrow {}^2A_{1g}$ transition. This value combined with the effective magnetic moment value, which is 1.6 µB, suggests a mononuclear Cu(II) complex in a square planar environment [46]. These results are confirmed by XRD.

3.2 Description of the structure of the complexes

3.2.1 Structure of the Manganese(III) complex

The complex crystallizes in the monoclinic system with the space group $P2_1/c$. The molecular structure of the manganese(III) complex (**1**) is given in Figure 1. Selected bond lengths and angles are listed in Table 4. The asymmetric unit contains one Mn^{3+} ion, one dideprotonated organic ligand and one chloride ion. The dideprotonated ligand acts in tetradentate fashion through two azomethine nitrogen atoms and two phenolate oxygen atoms. The coordination sphere around the Mn^{3+} ion is completed by a chloride ion. The Mn^{3+} ion is located in a N_2O_2Cl cavity. The environment of a pentacoordinated ion can be described using the Addison parameter $\tau = (\alpha - \beta)/60$, ($\alpha$ and β being the two largest angles around the metal: a value of $\tau = 0$ corresponds to a square-based pyramid geometry and a value of $\tau = 1$ designates a trigonal-based pyramid geometry) [49]. The τ value of 0.0078 is indicative of a distorted square pyramidal geometry. The basal plane of the polyhedron around the Mn1 ion is occupied by O1, O2, N1 and N2, while the apical position is occupied by Cl. The *cissoid* angles which are in the range [81.35(15)° – 92.51(12)°] and the *transoid* angle 162.89(16)° and 163.36(18)° deviate severely from the ideal values of 90° and 180°, respectively, as expected for a perfect square pyramidal geometry. All angles defined by the atom in the apical position with the atoms of the basal plane are in the range [95.82(12)°-100.43(11)°] and are far from the ideal value of 90°. The sum of the angle subtended by the atoms in the basal plane which is 355.6° is far from the ideal value of 360°. The square pyramidal environment around Mn1 is severely distorted. The Mn—O bond lengths [1.877(3) Á and 1.884(3) Á] are shorter than the Mn—N bond lengths [1.990(4) Á and 1.984(4) Á] due to the hard character of the phenolate oxygen. These values are comparable to the values observed for a similar Mn(III) complex [(salen)Mn^{III}Cl] [50]. The Mn-Cl bond [2.4252 (14) Á] is the longest and is comparable to the values reported for a similar complex [Mn(*L*)Cl] (H_2L is *N*,*N*'-Bis(5-allyl-3-methoxysalicylidene)ethylene-1,2-diamine) [51], due to the presence of a Jahn-Teller axial elongation [52]. The Mn(III) ion is situated 0.267 Å out of the plane defined by the four coordinated atoms of the ligand. After coordination the ligand forms two six-membered rings of MnOCCCN type and one five-membered ring of MnNCCN type. The six-membered rings form a dihedral angle of 3.60°. The five-membered ring forms a dihedral angle of 16.01° and 19.28°, respectively, with the two six-membered rings. The two phenyl groups of the ligand are twisted by each other forming a dihedral angle of 7.21°. Numerous non-classical intermolecular hydrogen bonds

of type C—H···Br (C15—H15···Br1^{v}, v = −*x*+1, *y*+1/2, −*z*+3/2; C3—H3···Br2^{vi}, vi = x−1, y, z; C5—H5···Br2^{vii}, vii = *x*−1, −*y*+1/2, *z*−1/2), C—H···Cl (C7—H7···Cl1^{iv}, iv = −*x*+1, −*y*, −*z*+1; C1A—H1A···Cl1^{viii}, viii = *x*, −*y*+1/2, *z*−1/2) and C—H···O (C10—H10B···O2^{viii}, viii = *x*, −*y*+1/2, *z*−1/2) consolidate the structure (Table 5, Figure 2). A Mn···O interaction between the Mn1 and O1 atoms from two different asymmetric units I is verified in the structure of the complex 1 (d Mn1···O1' = 2.968(3) Å), yielding a pseudo octahedral environment for the metal center.

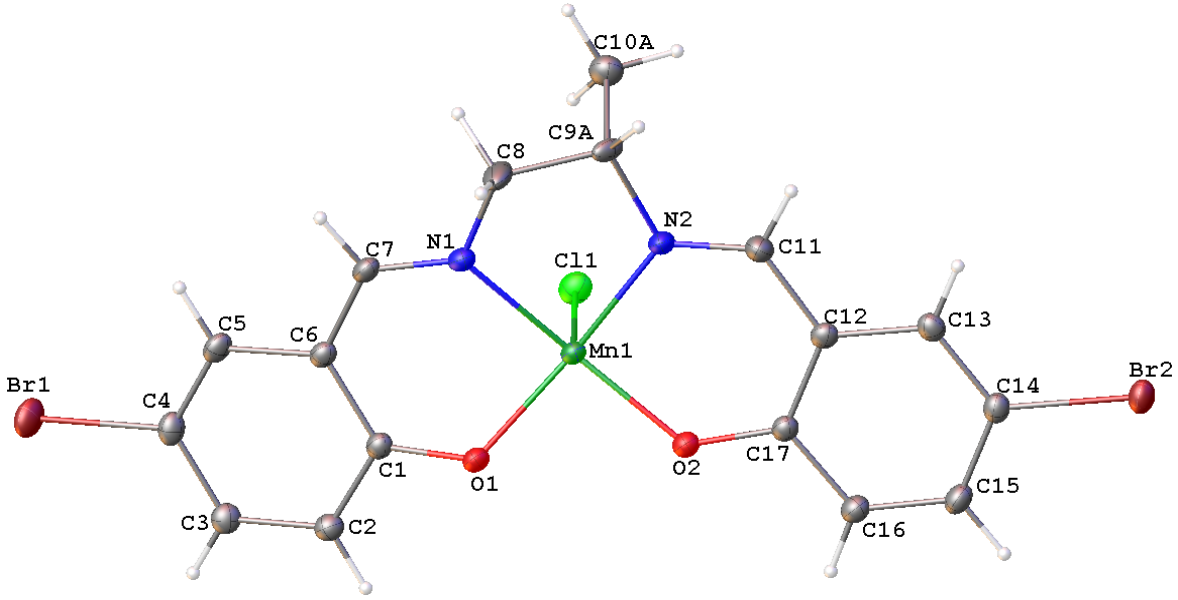

Figure 1. Crystal structure of the complex 1. Displacement ellipsoids are drawn at the 30% probability level.

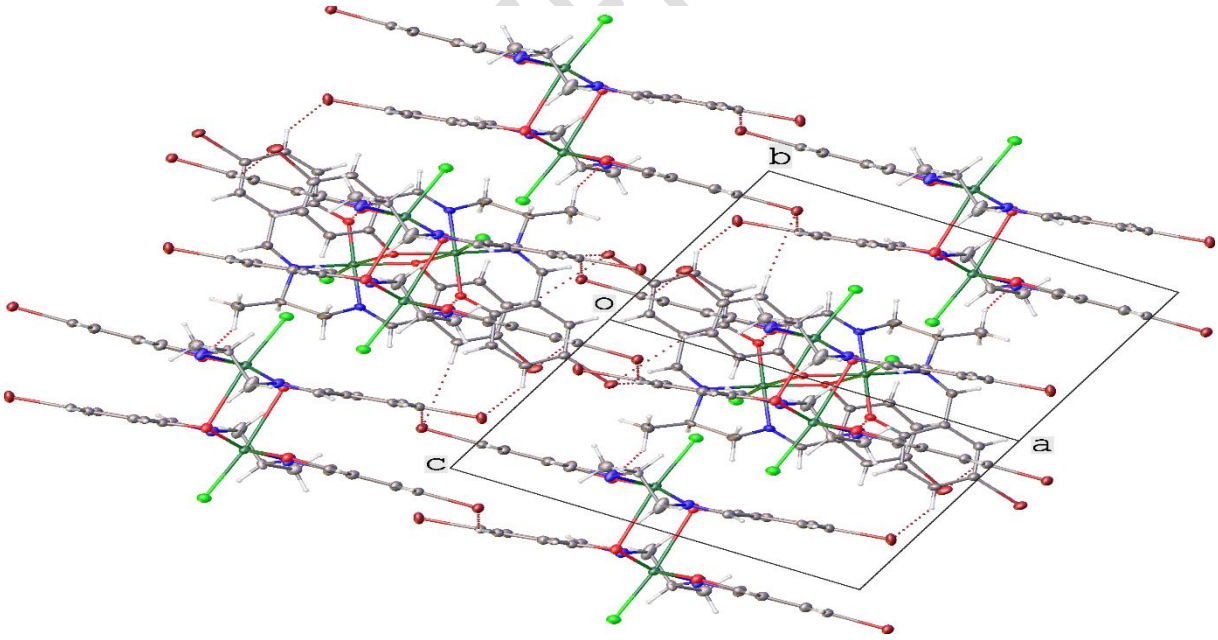

Figure 2. View of the packing in the *bc* plane of the compound in the crystal structure of 1.

3.2.2 Structure of the Copper(II) complex

The complex crystallizes in the monoclinic system with the space group C2/c. The molecular structure of the copper(II) complex (**5**) is given in Figure 3. Selected bond lengths and angles are listed in Table 4. The asymmetric unit contains one Cu^{2+} ion and one dideprotonated organic ligand. The Cu^{2+} ion is located in a N_2O_2 cavity. The metal center is tetracoordinated by the ligand through two imine nitrogen

atoms and two phenolate oxygen atoms. The environment around the Cu^{2+} ion can be characterized using the tetragonality parameter τ_4 [τ_4 = (360 - α - β)/141] (α and β being the largest angles around the central element, τ_4 = 0 designates a perfect square planar geometry and τ_4 = 1 gives a perfect tetrahedron) [47]. In the case of the [Cu(*L*)] complex the τ_4 value of 0.085 indicates a slightly distorted square planar geometry. The bond lengths Cu—O [1.902 (3) Å] and Cu—N [1.942(3) Å] are comparable to those found for a similar complex [Cu(*L*)] (H_2L = 4,4′-dibromo-2,2′-[cyclohexane-1,2-diylbis (nitrilomethanylylidene)]diphenol) in which Cu(II) is located in a square planar environment [48]. After coordination the ligand forms two six-membered rings of type CuOCCCN and one five-membered ring of type CuNCCN. The two six-membered rings (CuOCCCN) form a dihedral angle of 8.31°. The five-membered ring (CuNCCN) forms a dihedral angle of 10.47° with each of the six-membered rings. The two phenyl groups of the ligand are twisted relative to each other forming a dihedral angle of 11.68°. The values of the *cissoid* angles around Cu1 are in the range [84.3(2)°-93.68(13)°] with a sum of 360.55°, while the values of the *transoid* angles are identical and are worth 173.99(14)°. The values of these angles deviate slightly from the ideal values of the angles which are 90° and 180° for perfect square planar geometry. The ligand is chiral with a methyl substituent on the aliphatic chain. The structure is composed of two asymmetric molecules oriented in opposite directions. All the atoms are perfectly superimposed except the methyl substituent which is responsible for the asymmetry of the ligand. The consequence is that the carbon atom carrying the methyl substituent of the second molecule will be superimposed on the -CH_2- carbon atom of the first molecule thus giving the structure illustrated in figure 3. Scheme 2 shows the superposition process. Weak intermolecular bond of type C—H···Br (C3—H3···Br1^{i}, I = −*x*+3/2, *y*−1/2, −*z*+3/2; C7—H7···Br1^{ii}, ii = −*x*+3/2, *y*+1/2, −*z*+3/2) and C—H···O (C8—H8A···O^{iii}, iii = −*x*+1, −*y*+1, −*z*+1) consolidate the structure (Table 5, Figure 4)

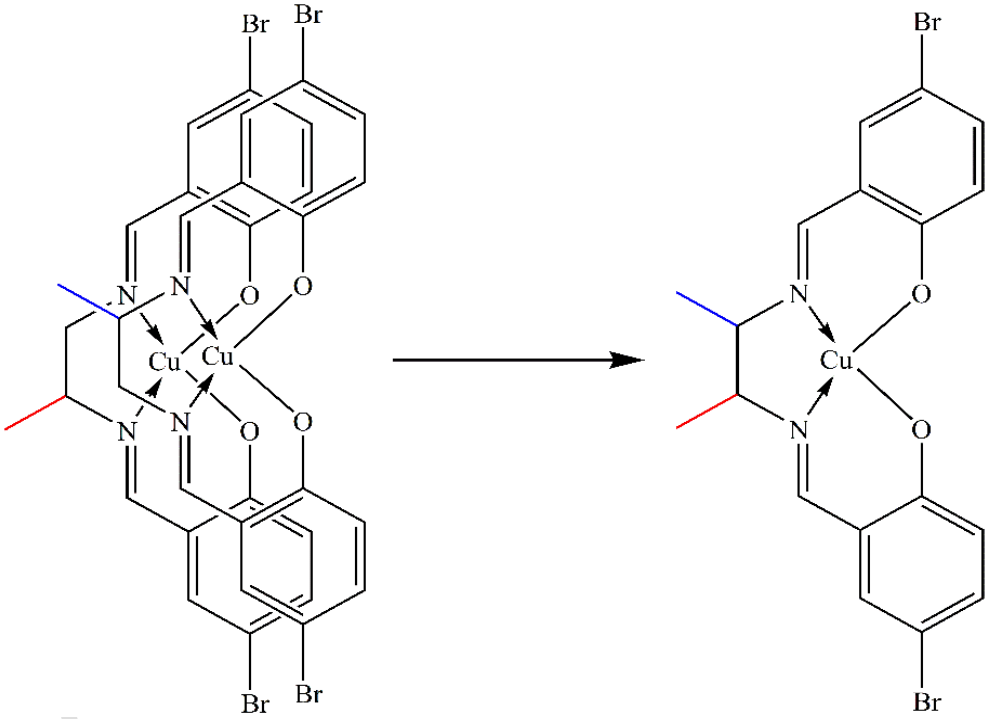

Scheme 2. Superposition of the molecules oriented in opposite directions.

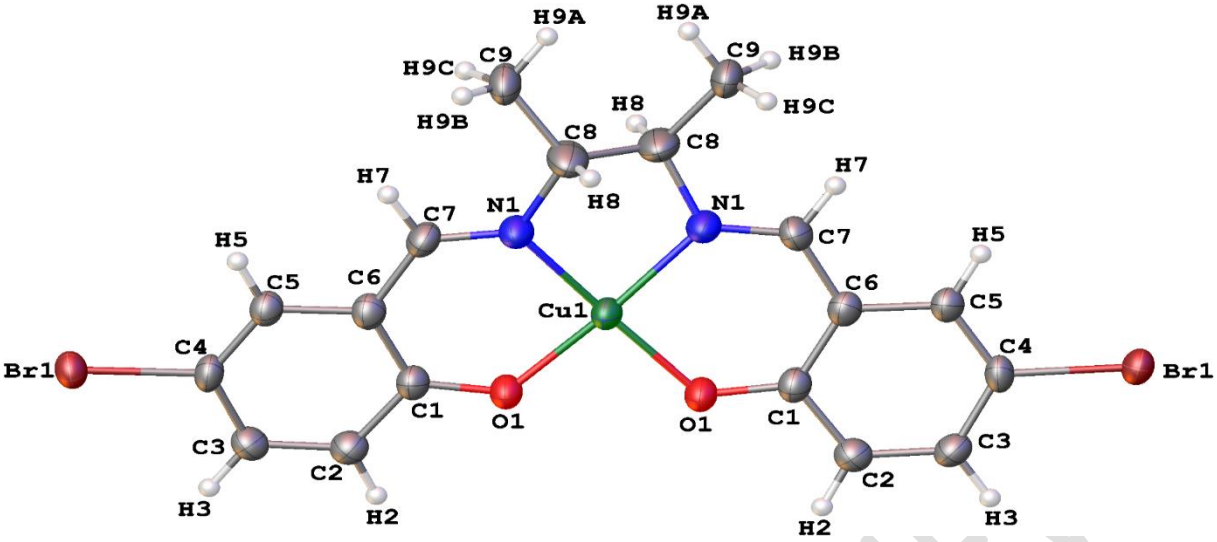

Figure 3. Crystal structure of complex 5. Displacement ellipsoids are drawn at the 30% probability level.

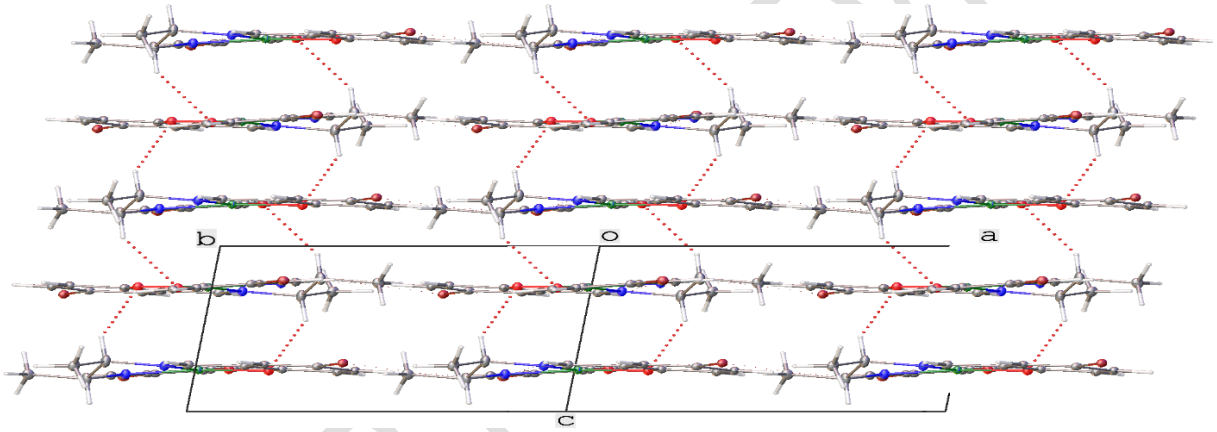

Figure 4. View of the packing in the *ab* plane of the compound in the crystal structure of 5.

Table 4. Selected bond lengths and bond angles the complexes 1 and 5.

1		5	
Mn1—Cl1	2.4252 (14)	Cu1—O1^{i}	1.902 (3)
Mn1—O2	1.877 (3)	Cu1—O1	1.902 (3)
Mn1—O1	1.884 (3)	Cu1—N1^{i}	1.942 (3)
Mn1—N1	1.990 (4)	Cu1—N1	1.942 (3)
Mn1—N2	1.984 (4)	N1—C7	1.283 (5)
N1—C7	1.273 (6)	N1—C8	1.480 (5)
N1—C8	1.465 (6)		
O2—Mn1—Cl1	100.43 (11)	O1^{i}—Cu1—O1	88.87 (17)
O2—Mn1—O1	92.51 (12)	O1—Cu1—N1	93.68 (13)
O2—Mn1—N1	162.89 (16)	O1^{i}—Cu1—N1	173.99 (14)
O2—Mn1—N2	91.52 (14)	O1^{i}—Cu1—N1^{i}	93.68 (13)
O1—Mn1—N1	90.24 (14)	O1—Cu1—N1^{i}	173.99 (14)
O1—Mn1—N2	163.36 (18)	N1^{i}—Cu1—N1	84.3 (2)
N2—Mn1—N1	81.35 (15)		
(i) −*x*+1, −*y*+1, −*z*+1.		(i) −*x*+1, *y*, −*z*+3/2.	

Table 5. Hydrogen-bond geometry for complex 4 and 1.

D—H···*A*	*D*—H	H···*A*	*D*···*A*	*D*—H···*A*
		[CuL]		
C3—H3···Br1^{i}	0.95	3.00	3.821 (4)	146.1
C7—H7···Br1^{ii}	0.95	3.13	4.023 (4)	158.2
C8—H8A···O1^{iii}	1.00	2.45	3.348 (7)	149.2
		[MnLCl]		
C7—H7···Cl1^{iv}	0.94	2.98	3.497 (4)	116.3
C15—H15···Br1^{v}	0.94	3.12	3.798 (5)	130.5
C3—H3···Br2^{vi}	0.94	3.05	3.841 (5)	142.3
C5—H5···Br2^{vii}	0.94	3.00	3.930 (4)	171.6
C9—H9···Cl1	0.99	2.92	3.514 (11)	119.8
C10—H10B···O2^{viii}	0.97	2.50	3.242 (11)	132.9
C1A—H1A···Cl1^{viii}	0.99	2.87	3.641 (12)	135.8

Symmetry codes: (i) −*x*+3/2, *y*−1/2, −*z*+3/2; (ii) −*x*+3/2, *y*+1/2, −*z*+3/2; (iii) −*x*+1, −*y*+1, −*z*+1 , (iv) −*x*+1, −*y*, −*z*+1; (v) −*x*+1, *y*+1/2, −*z*+3/2; (vi) *x*−1, *y*, *z*; (vii) *x*−1, −*y*+1/2, *z*−1/2; (viii) *x*, −*y*+1/2, *z*−1/2.

4. CONCLUSION

The ligand *N*,*N*'-Bis(5-bromosalicylidene)-(2-methyl)ethane-1,2-diamine was synthetized and structurally characterized. The ligand was used for chelation with transition metal ions such as Co(II), Fe(II), Mn(II), Ni(II) and Cu(II) ions. The complexes are characterized by FTIR and UV-Vis spectroscopies, room temperature magnetic moments measurements, conductivity measurement and X-ray diffraction for the Mn(III) and Cu(II) complexes. The ligand acts as dinegative tetradentate in all complexes. In each complex the ligand molecule coordinates the metal ion through two nitrogen azomethine atoms and two phenolate oxygen atoms. On the basis of the analytical data, the cobalt (II) complex shows octahedral geometry, nickel and copper(II) complexes show square planar geometries, while iron(III) and manganese(III) complexes show square pyramidal geometries. The X-ray structures determination of the copper and the manganese complexes confirm the geometries deduced from the UV-visible, the magnetic moments measurements and the conductivity data.

5. SUPPLEMENTARY DATA

CCDC– 2408375 and 2408376 contain the supplementary crystallographic data for the complex **5** and **2**. These data can be obtained free of charge via www.ccdc.cam.ac.uk/conts/retrieving.html, or from the Cambridge Crystallographic Data Centre, 12 Union Road, Cambridge CB2 1EZ, UK (Telephone: +44–01223–762910; Fax: +44–1223–336033; or E-mail: xxxxx@ccdc.cam.ac.uk).

References

1. Zhang Y, Du M-X, La Y-T, Yan Y-J, Dong, W-K. (2024). Synthesis, structural characterizations and theoretical calculations of the Ni(II) complex based on a novel Salamo-Salen-Salamo-type hybrid ligand. Journal of Molecular Structure, 1296, 136841.
Available: https://doi.org/10.1016/j.molstruc.2023.136841

2. Karmakar M, Das, R, Chattopadhyay S. (2024). A comprehensive overview of the synthesis, structure, and application of azide bridged manganese(III) complexes with salen type Schiff base blocking ligands. Inorganica Chimica Acta, 569, 122106.
Available: https://doi.org/10.1016/j.ica.2024.122106
3. Middya P, Das S, Chattopadhyay S. (2025). An overview of the synthesis, structure and different applications of hetero-nuclear complexes of different transition metals and sodium with salen type compartmental ligands. Inorganica Chimica Acta, 574, 122405.
Available: https://doi.org/10.1016/j.ica.2024.122405
4. Bhunia S, Chattopadhyay S. (2025). A brief overview on the chemistry of trinuclear complexes of cobalt with salen type tetradentate N_2O_2-donor Schiff base ligands and their reduced analogous. Inorganica Chimica Acta, 577, 122475.
Available: https://doi.org/10.1016/j.ica.2024.122475
5. McCabe CA, Mitchell AL, Bonitatibus PJ, Dinolfo PH. (2025). Ligand-dependent redox-coupled spin crossover of a five coordinate cobalt salen complex. Inorganica Chimica Acta, 577, 122459.
Available: https://doi.org/10.1016/j.ica.2024.122459
6. Belal DM, El-Ayaan UI, El-Gamil MM, Younis AM, El-Reash GMA. (2023). Fluorescence, cyclic voltammetric, computational, and spectroscopic studies of Mn(II), Co(II), Pd(II), Zn(II) and Cd(II) complexes of salen ligand and their biological applications. Journal of Molecular Structure, 1271, 134142.
Available: https://doi.org/10.1016/j.molstruc.2022.134142
7. Asadollahi P, Bikas R, Krawczyk MS, Lis T. (2022). Catalytic oxidation of styrene by dinuclear Mn(III) coordination compound with asymmetric tridentate half-Salen type NNO-donor ligand. Polyhedron, 211, 115537.
Available: https://doi.org/10.1016/j.poly.2021.115537
8. Feng X, Xu Z, Zhao J, Hansen HA, Deng Q. (2022). Role of macrocyclic salen-type Schiff base ligands in one-dimensional Co(II) complexes for superior activities toward oxygen reduction/evolution reactions. International Journal of Hydrogen Energy, 47(63), 27000–27011.
Available: https://doi.org/10.1016/j.ijhydene.2022.06.055
9. Chakrabortty S, de Bruin B, de Vries JG. (2024). Cobalt-Catalyzed Asymmetric Hydrogenation: Substrate Specificity and Mechanistic Variability. Angewandte Chemie International Edition, 63(10), e202315773.
Available: https://doi.org/10.1002/anie.202315773
10. Nguyen ZA, Minteer SD (2024). Utility of Immobilized Metal Salens as Electrocatalysts: Fuel Cells and Organic Electrosynthesis. ChemElectroChem, 2024, e202400445.
Available: https://doi.org/10.1002/celc.202400445
11. Yao X, Qiu M, Lü W, Chen H, Zheng Z. (2001). Substituted salen–Ru(II) complexes as catalysts in the asymmetric cyclopropanation of styrene by ethyl diazoacetate: the influence of substituents and achiral additives on activity and enantioselectivity. Tetrahedron: Asymmetry, 12(2), 197–204.
Available: https://doi.org/10.1016/S0957-4166(01)00014-3
12. Ghaffari A, Behzad M, Pooyan M, Rudbari HA, Bruno G. (2014). Crystal structures and catalytic performance of three new methoxy substituted salen type nickel(II) Schiff base complexes derived from meso-1,2-diphenyl-1,2-ethylenediamine. Journal of Molecular Structure, 1063, 1–7.
Available: https://doi.org/10.1016/j.molstruc.2014.01.052
13. Middya P, Saha A, Chattopadhyay S. (2023). A comprehensive overview on the synthesis, structures and applications of mono-nuclear transition metal complexes with asymmetrically substituted ‘salen-type’ Schiff bases. Inorganica Chimica Acta, 545, 121246.
Available: https://doi.org/10.1016/j.ica.2022.121246
14. Mandal U, Rizzoli C, Chakraborty B, Karmakar S, Mandal S, Bandyopadhyay D. (2024). Synthesis, crystal structure, and characterization of two new end-to-end 1D pseudohalide bridged manganese(III) complexes. Transition Metal Chemistry, 49(3), 137–147.
Available: https://doi.org/10.1007/s11243-023-00569-0
15. Lin Y-W. (2024). Functional metalloenzymes based on myoglobin and neuroglobin that exploit covalent interactions. Journal of Inorganic Biochemistry, 257, 112595.
Available: https://doi.org/10.1016/j.jinorgbio.2024.112595
16. Li J, Ren Y, Qi C, Jiang H. (2017). A chiral salen-based MOF catalytic material with high thermal, aqueous and chemical stabilities. Dalton Transactions, 46(24), 7821–7832.
Available: https://doi.org/10.1039/C7DT01116D

17. Ying P, Ying T, Chen H, Xiang K, Su W, Xie H, Yu J. (2024). Iron-catalyzed asymmetric Csp3–H/Csp3–H coupling: improving the chirality induction by mechanochemical liquid-assisted grinding. Organic Chemistry Frontiers, 11(1), 127–134.
Available: https://doi.org/10.1039/D3QO01467C
18. Ji L, Wang J, Li Z, Zhu X, Hu P. (2024). Chiral Star-Shaped [CoIII3LnIII] Clusters with Enantiopure Schiff Bases: Synthesis, Structure, and Magnetism. Molecules, 29(14), 3304. Available: https://doi.org/10.3390/molecules29143304
19. Yao J-L, Li Z. (2024). Hafnium(IV)-Salen-Catalyzed Highly Reactive and Enantioselective Epoxidation Directed by Amides. ACS Catalysis, 14(16), 12494–12499.
Available: https://doi.org/10.1021/acscatal.4c03648
20. Raptopoulou C. P. (2024). Chiral 4f and 3d-4f Complexes from Enantiopure Salen-Type Schiff Base Ligands. Crystals 14(5), 474.
Available: https://doi.org/10.3390/cryst14050474
21. La Y-T, Yan Y-J, Li X, Zhang Y, Sun Y-X, Dong W-K. (2024). A novel Salamo-Salen-Salamo hybrid Mg(II) complex fluorescent chemosensor for highly effective monitoring $H_2PO_4^-$ in Zebrafish and plants. Journal of Molecular Structure, 1295, 136641.
Available: https://doi.org/10.1016/j.molstruc.2023.136641
22. Alfonso-Herrera L A, Hernández-Romero D, Cruz-Navarro JA, Ramos-Ligonio Á, López-Monteon A, Rivera-Villanueva JM, Morales-Morales D, Colorado-Peralta, R. (2024). Transition metal complexes with tetradentate Schiff bases (N_2O_2) obtained from salicylaldehyde: A review of their possible anticancer properties. Coordination Chemistry Reviews, 505, 215698.
Available: https://doi.org/10.1016/j.ccr.2024.215698
23. Todarwal MA, Sancheti RS, Nikume SR, Patel HM, Bendre RS. (2024). Anti-Malarial and Multi-Bioactive Co (II), Cu (II) and Ni (II) Salen Complexes: Synthesis, Characterization and Computational Studies. Chemistry Biodiversity, 21(9), e202400715.
Available: https://doi.org/10.1002/cbdv.202400715
24. Bufarwa S, El-Seifat R, Binhamad H, Hesien R. (2024). Synthesis, characterization, thermal, theoretical studies, antimicrobial, antioxidant activity, superoxide dismutase-like activity and catalase mimetics of metal(II) complexes derived from sugar and Schiff base. Reviews in Inorganic Chemistry, 44(4), 521–533.
Available: https://doi.org/doi:10.1515/revic-2023-0028
25. Kaplan E, Koc ZE, Uysal A, Uba AI, Zengin G. (2024). Elucidation of the Microwave-Assisted Synthesis and Characterization of Heteronuclear Complexes of Bisbenzimidazole Derivatives and Their Biological Activities by In Vitro and In Silico Assays. Chemical Biology Drug Design, 104(3), e14605.
Available: https://doi.org/10.1111/cbdd.14605
26. Kyoya Y, Takahashi K, Kosaka W, Huang R-K, Xue C, Wu J, Miyasaka H, Nakamura, T. (2024). Unlocking single molecule magnetism: a supramolecular strategy for isolating neutral Mn^{III} salen-type dimer in crystalline environments. Dalton Transactions, 53(17), 7517–7521.
Available: https://doi.org/10.1039/D4DT00323C
27. Ikeshita M, Kuroda A, Suzuki S, Imai Y, Tsuno T. (2024). Switching of Circularly Polarized Luminescence via Dynamic Axial Chirality Control of Chiral Bis(Boron Difluoride) Complexes with Salen Ligands. ChemPhotoChem, 8(10), e202400110.
Available: https://doi.org/10.1002/cptc.202400110
28. Boruah SK, Das H, Boruah PK. (2024). Optical and electrochemical investigation on one-step three electron reduction of [AuIII(Salen)]Cl to Au(0): a comprehensive analysis. Journal of the Iranian Chemical Society, 21(7), 1937–1945.
Available: https://doi.org/10.1007/s13738-024-03039-1
29. Sheldrick GM. (2015). SHELXT – Integrated space-group and crystal-structure determination. Acta Crystallographica Section A, 71(1), 3–8.
Available: https://doi.org/10.1107/S2053273314026370
30. Sheldrick GM. (2015). Crystal structure refinement with SHELXL. Acta Crystallographica Section C, 71(1), 3–8.
Available: https://doi.org/10.1107/S2053229614024218
31. Farrugia LJ. (2012). WinGX and ORTEP for Windows: an update. Journal of Applied Crystallography, 45(4), 849–854.
Available: https://doi.org/10.1107/S0021889812029111
32. Tohidiyan Z, Sheikhshoaie I, Khaleghi M, Mague JT. (2017). A novel copper (II) complex containing a tetradentate Schiff base: Synthesis, spectroscopy, crystal structure, DFT study,

biological activity and preparation of its nano-sized metal oxide. Journal of Molecular Structure, 1134, 706–714.
Available: https://doi.org/10.1016/j.molstruc.2017.01.026
33. Mohan N, Sreejith SS, George R, Mohanan PV, Kurup MRP. (2021). Synthesis, crystal structure and ligand based catalytic activity of octahedral salen Schiff base Co(III) compounds. Journal of Molecular Structure, 1229, 129779.
Available: https://doi.org/10.1016/j.molstruc.2020.129779
34. Kargar H, Torabi V, Akbari A, Behjatmanesh-Ardakani R, Sahraei A, Tahir MN. (2020). Pd(II) and Ni(II) complexes containing an asymmetric Schiff base ligand: Synthesis, x-ray crystal structure, spectroscopic investigations and computational studies. Journal of Molecular Structure, 1205, 127642.
Available: https://doi.org/10.1016/j.molstruc.2019.127642
35. Pervaiz M, Ahmad I, Yousaf M, Kirn S, Munawar A, Saeed Z, Adnan A, Gulzar T, Kamal T, Ahmad A, Rashid A. (2019). Synthesis, spectral and antimicrobial studies of amino acid derivative Schiff base metal (Co, Mn, Cu, and Cd) complexes. Spectrochimica Acta Part A: Molecular and Biomolecular Spectroscopy, 206, 642–649.
Available: https://doi.org/10.1016/j.saa.2018.05.057
36. Saghatforoush LA, Hosseinpour S, Bezpalko MW, Kassel WS. (2019).Inorganica Chimica Acta, 484, 527–534.
Available: https://doi.org/10.1016/j.ica.2018.04.053
37. Geary WJ. (1971). The use of conductivity measurements in organic solvents for the characterisation of coordination compounds. Coordination Chemistry Reviews, 7(1), 81–122.
Available: https://doi.org/10.1016/S0010-8545(00)80009-0
38. Siddiqi ZA, Kumar S, Khalid M, Shahid M. (2009). Spectral studies of Fe(III) complexes of dipodal tridentate chelating agents. Spectrochimica Acta Part A: Molecular and Biomolecular Spectroscopy, 71(5), 1845–1850.
Available: https://doi.org/10.1016/j.saa.2008.07.016
39. Seck GA, Guèye MN, Tamboura FB, Thiam IE, Diouf O, Sall AS, Gaye M. (2024). Synthesis and Characterization of Binuclear Complexes of Metals Transition of N'1,N'4-Bis(1-(Pyridin-2-yl)Ethylidene)Succinohydrazide. International Research Journal of Pure and Applied Chemistry, 25(5), 111–122.
Available: https://doi.org/10.9734/irjpac/2024/v25i5879
40. Yadav P, Jakubaszek M, Spingler B, Goud B, Gasser G, Zelder F. (2020). Fe^{III}–Salen-Based Probes for the Selective and Sensitive Detection of E450 in Foodstuff. Chemistry – A European Journal, 26(25), 5717–5723.
Available: https://doi.org/10.1002/chem.201905686
41. Fleck M, Layek M, Saha R, Bandyopadhyay D. (2013). Synthetic aspects, crystal structures and antibacterial activities of manganese(III) and cobalt(III) complexes containing a tetradentate Schiff base. Transition Metal Chemistry, 38(7), 715–724.
Available: https://doi.org/10.1007/s11243-013-9741-5
42. Korupoju SR, Mangayarkarasi N, Ameerunisha S, Valente EJ, Zacharias PS. (2000). Formation of dinuclear macrocyclic and mononuclear acyclic complexes of a new trinucleating hexaaza triphenolic Schiff base macrocycle: structure and NLO properties. Journal of the Chemical Society, Dalton Transactions, (16), 2845–2852.
Available: https://doi.org/10.1039/B002700F
43. Singh K, Thakur R, Kumar V. (2016). Co(II), Ni(II), Cu(II), and Zn(II) complexes derived from 4-[3-(4-bromophenyl)-1-phenyl-1H-pyrazol-4-ylmethylene-amino]-3-mercapto-6-methyl-5-oxo-1,2,4-triazine. Beni-Suef University Journal of Basic and Applied Sciences, 5(1), 21–30.
Available: https://doi.org/10.1016/j.bjbas.2016.02.001
44. Torabi V, Kargar H, Akbari A, Behjatmanesh-Ardakani R, Amiri Rudbari H, Nawaz Tahir M. (2018). Nickel(II) complex with an asymmetric tetradentate Schiff base ligand: synthesis, characterization, crystal structure, and DFT studies. Journal of Coordination Chemistry, 71(22), 3748–3762.
Available: https://doi.org/10.1080/00958972.2018.1521967
45. Hernández-Molina R, Mederos A, Gili P, Domínguez S, Núñez P, Germain G, Debaerdemaeker T. (1997). Coordinating ability in DMSO-water 80:20 wt./wt. of the Schiff base N,N′-3,4-toluenebis(salicylideneimine) with divalent cations. Crystal structure of the nickel(II) complex. Inorganica Chimica Acta, 256(2), 319–325.
Available: https://doi.org/10.1016/S0020-1693(96)05440-0

46. Subramanian PS, Suresh E, Srinivas D. (2000). Synthesis, X-ray Structure, Single-Crystal EPR and ^{1}H NMR Studies of a Distorted Square Planar $Cu(salEen)_2(ClO_4)_2$ Complex in a Novel Bilayered Architecture: salEen = N,N-Diethylethylenesalicylidenamine. Inorganic Chemistry, 39(10), 2053–2060.
Available: https://doi.org/10.1021/ic990874q
47. Yang L, Powell DR, Houser RP. (2007). Structural variation in copper(i) complexes with pyridylmethylamide ligands: structural analysis with a new four-coordinate geometry index, $\tau 4$. Dalton Transactions, (9), 955–964.
Available: https://doi.org/10.1039/B617136B
48. Tohidiyan Z, Sheikhshoaie I, Khaleghi M, Mague JT. (2017). A novel copper (II) complex containing a tetradentate Schiff base: Synthesis, spectroscopy, crystal structure, DFT study, biological activity and preparation of its nano-sized metal oxide. Journal of Molecular Structure, 1134, 706–714.
Available: https://doi.org/10.1016/j.molstruc.2017.01.026
49. Addison AW, Rao TN, Reedijk J, van Rijn J, Verschoor GC. (1984). Synthesis, structure, and spectroscopic properties of copper(II) compounds containing nitrogen–sulphur donor ligands; the crystal and molecular structure of aqua[1,7-bis(N-methylbenzimidazol-2′-yl)-2,6-dithiaheptane]copper(II) perchlorate. Journal of the Chemical Society, Dalton Transaction, (7), 1349–1356.
Available: https://doi.org/10.1039/DT9840001349
50. Scheurer A, Puchta R, Hampel F. (2010). X-ray structure analysis and DFT study of a chiral (salen)MnIII complex toward understanding of inversion of enantioselection in epoxidation catalysts. Journal of Coordination Chemistry, 63(14–16), 2868–2878.
Available: https://doi.org/10.1080/00958972.2010.508520
51. Liu D, Zhang Z, Zhang X, Lü X. (2016). Alternating Ring-Opening Copolymerization of Cyclohexene Oxide and Maleic Anhydride with Diallyl-Modified Manganese(III)–Salen Catalysts. Australian Journal of Chemistry, 69(1), 47–55.
Available: https://doi.org/10.1071/CH15162
52. Feng Y, Wang C, Zhao Y, Li J, Liao D, Yan S, Wang Q. (2009). Out-of-plane dimeric Mn^{III} quadridentate Schiff-base complexes: Synthesis, structure and magnetic properties. Inorganica Chimica Acta, 362(10), 3563–3568.
Available: https://doi.org/10.1016/j.ica.2009.03.048